Formation Flying for Distributed InSAR

Daniel P. Scharf,* Emmanuell A. Murray,† Scott R. Ploen,*
Konstantin G. Gromov,‡ and Curtis W. Chen§
Jet Propulsion Laboratory, California Institute of Technology, Pasadena, CA, 91109-8099, USA

We consider two spacecraft flying in formation to create an interferometric synthetic aperture radar (InSAR). Several candidate orbits for such an InSAR formation have been previously determined based on radar performance and Keplerian orbital dynamics. However, without active control, disturbance-induced drift can degrade radar performance and (in the worst case) cause a collision. This study evaluates the feasibility of operating the InSAR spacecraft as a formation, that is, with inter-spacecraft sensing and control. We describe the candidate InSAR orbits, design formation guidance and control architectures and algorithms, and report the Δv and control acceleration requirements for the candidate orbits for several tracking performance levels. As part of determining formation requirements, a formation guidance algorithm called Command Virtual Structure is introduced that can reduce Δv requirements compared to standard Leader/Follower formation approaches. In addition, an orbit maintenance and formation reconfiguration guidance algorithm is developed for changing both relative orbits and the overall formation orbit.

I. Introduction

In distributed interferometric synthetic aperture radar (InSAR), at least two synthetic aperture radar spacecraft obtain additional information by differencing radar phase information from multiple viewpoints of the same target. InSAR can be used used to generate digital elevation maps (e.g., Shuttle Radar Topography Mission[1]) or measure surface velocities for geology and climatology (e.g., tectonic[2] or glacial[3] movement). Since arbitrary spacecraft motions in LEO are impractical,[4] thrust-free orbits are designed in simplified dynamics models to generate desirable relative spacecraft motion (i.e., InSAR baselines). The resulting relative motion is referred to as a passive relative orbit (PRO).[5,6]

As part of an on-going formation InSAR study, several candidate Keplerian PROs have been selected for a two-spacecraft InSAR. Since the minimum altitude for the InSAR formation is 500 km and the two InSAR spacecraft are essentially identical, the principal disturbance on the formation is the first zonal harmonic of Earth oblateness, J_2.[a] The spacecraft must be actively controlled to prevent J_2-induced drift from degrading InSAR performance or, in the worst case, causing collision.

We consider formation flying InSAR, that is, explicitly controlling the relative spacecraft position by coupling the spacecraft through an automatic control law. This paper presents the results of a two-spacecraft, formation flying InSAR study. Our focus is on formation flying requirements and not on radar performance. Specifically, the study determines the Δv and control acceleration requirements of several candidate InSAR PROs for several levels of performance. A sensitivity analysis with respect to control design parameters is also included. This analysis shows that the maximum acceleration required by the controller to maintain the formation can be tailored to the desired level.

As part of the formation InSAR study, a new formation guidance algorithm called Command Virtual Structure (CVS) has been developed. CVS, a type of Leader/Follower formation architecture,[8] can reduce

§Senior Engineer, Guidance and Control Analysis Group, Member AIAA.
§Associate Engineer, Guidance and Control Analysis Group.
§Staff Engineer, Guidance and Control Analysis Group.
§Senior Engineer, Radar System Engineering and Algorithm Development Group

[a]Based on Ref. 7, a reasonable value of $C_D A/m$ (i.e., the inverse ballistic coefficient) for a SAR spacecraft is 0.0043 m^2/kg. In addition, the GRACE mission, which consists of two identical spacecraft separated by 220 km, has observed ballistic coefficient differences of 1%.[7] For a 520 km altitude orbit, these facts result in a maximum differential drag acceleration of $2e{-}9$ m/s^2. At the same altitude for spacecraft separated by 300 m, the maximum differential acceleration due to J_2 is $4e{-}6$ m/s^2.

Δv requirements by up to an order of magnitude compared to standard Leader/Follower implementations. Additionally, a formation guidance algorithm has been developed for changing both the spacecraft's relative orbit and the overall formation orbit. This orbit maintenace/reconfigur atoin (OM/R) algorithm is an extension of standard formation linear programming approaches[9] to more general boundary conditions.

Previous work in InSAR formations has focused on PRO design.[5,10,11] In Refs. 7, 12 and 13, open loop Δv estimates are given to cancel differential aerodynamic drag and differential mean J_2. While there is considerable research in closed-loop formation control,[14] the majority of LEO formation work has focused on showing stability or performance; not on determining Δv requirements as a function of performance. Several near-optimal orbit transfer methodologies have been developed for application in model predictive control laws. See Ref. 15 and references therein. However, sensor noise and actuation errors can limit model predictive control performance to tens of meters.[16] Previous studies of Δv requirements for precision formation flying (i.e., better than 10 meter tracking performance) include Refs. 9, 17 and 18. These earlier studies considered a single PRO and a selection of control architectures. In addition to introducing the CVS and OM/R formation guidance algorithms, this paper extends these earlier studies by considering a spectrum of InSAR-relevant PROs for several levels of performance and control designs.

The paper is organized as follows. In Section II, four classes of InSAR-relevant PROs are reviewed briefly. A new PRO called the pseudo-frozen corkscrew is introduced. Additionally, we discuss the PRO parameterization methodology used in the formation guidance algorithms. Next, the overall control architecture and control algorithm design methodology are presented in Section III. Then two formation guidance algorithms, the new CVS architecture and a standard Leader/Follower architecture called Prescribed-ν, are developed in Section IV. In Section V, the simulation environment used to evaluate formation Δv and acceleration requirements is briefly described, including assumptions on sensor noise and disturbances. The main results of this paper, requirements for Δv and acceleration and the sensitivity of these requirements to control design parameters, are given in Section VI. Section VII presents the OM/R algorithm and representative Δv requirements for changing PROs. Additionally, the OM/R algorithm is validated against a Hohmann transfer. Finally, we summarize and identify areas for future study.

In the sequel, we refer to the two InSAR spacecraft as SC_1 and SC_2. SC_1 is considered the Leader, but in implementation, the roles of the spacecraft would be switched to balance fuel. Regarding nomenclature, column vectors are given in bold and estimated values have a carat symbol (e.g., $\hat{\boldsymbol{\rho}}$ is the estimated relative position vector).

II. InSAR Passive Relative Orbits

In this section, the four classes of InSAR PROs are described. Relative motion is characterized in the rotating Local-Vertical, Local-Horizontal (LVLH) frame, which is defined as follows. The origin can be either a physical spacecraft or a prescribed location in space. The x-axis is along the position vector of the spacecraft (or prescribed point) with respect to the Earth, the z-axis is along the angular momentum vector, and the y-axis completes the triad. For a circular orbit, the y-axis is parallel to the velocity. The x-, y- and z-axes are also referred to as radial, along-track, and cross-track. Unless otherwise noted, the orbit of SC_1 is the basis for the LVLH frame.

The four classes of PROs that are being considered in the overall InSAR study are referred to as (i) cartwheel, (ii) corkscrew, (iii) pseudo-frozen corkscrew, and (iv) pendulum. Three of the classes are well-known,[19] but the pseudo-frozen corkscrew (conceived by C.W. Chen) is new as far as the authors could determine. For each of these PRO classes, different altitudes and InSAR baseline lengths are considered. For all PROs, the two spacecraft have identical semi-major axes, as this is a necessary condition for periodic relative motion.[20] Relations in this section were derived using Keplerian orbit geometry and projecting relative motion into InSAR baselines.

The cartwheel PRO consists of relative motion in the orbit plane. It is produced by placing two spacecraft on equally eccentric orbits with arguments of periapsis and initial true anomalies both 180° apart. This phasing gives a maximum radial separation (i.e., baseline) of

$$B_r = 2ae\,, \tag{1}$$

where a and e are the semi-major axis and eccentricity of the two orbits. The inclinations and longitude of the ascending nodes are identical.

The corkscrew PRO begins with a cartwheel and then rotates the orbit of SC_2 about the periapsis vector

of SC_1's orbit, producing a cross-track separation. The angle of rotation θ_p determines the cross-track baseline via

$$B_c = a(1-e^2)\sin(\theta_p)\,. \tag{2}$$

The semilatus rectum $p = a(1-e^2)$, not the semi-minor axis $a\sqrt{(}1-e^2)$, gives the maximum cross track baseline due to phasing within the two orbits. For a corkscrew PRO, both B_r and B_c must be specified. Depending on the argument of periapsis of SC_1, the periapsis rotation for a near-polar orbit produces a differential inclination, a differential longitude of the ascending node, or a combination thereof.

The pseudo-frozen corkscrew PRO partially compensates for J_2- and J_3-induced variations. First, for the desired semi-major axis and inclination, the frozen orbit argument of periapsis ω_f and eccentricity e_f are calculated. See Ref. 21. The frozen values eliminate long period variations of eccentricity and argument of periapsis. The frozen eccentricity is given by

$$e_f = -\frac{1}{2}\frac{J_3}{J_2}\frac{R_\oplus}{a}\sin i \sin\omega_f\,, \tag{3}$$

where $R_\oplus$ is the mean equatorial radius of the Earth, and recall J_2 and J_3 have opposite signs. Both SC_1 and SC_2 have an ω_f of 90°. Since the arguments of periapsis are identical, the spacecraft must have different eccentricities to obtain the radial baseline of the regular corkscrew. It can be shown that a differential eccentricity of

$$\Delta e = B_{r,f}/a \tag{4}$$

gives the desired horizontal baseline. Hence, SC_1 and SC_2 are given eccentricities of $e_f+\Delta e/2$ and $e_f-\Delta e/2$, respectively. Finally, to obtain the vertical baseline the orbits are again rotated about their common periapsis vector. However, Eq. (2) must be modified to

$$B_{c,f} = 2a(1-e_f^2-\Delta e^2)\sin(\theta_p)\,. \tag{5}$$

The orbit of SC_1 and SC_2 are then rotated $\theta_p/2$ and $-\theta_p/2$ about their common periapsis vector.

The pendulum PRO is produced by rotating two identical orbits about their periapsis vector, giving a vertical baseline via Eq. (2). We use circular orbits, and define the argument of periapsis to be zero. To avoid collisions, the initial true anomalies of the orbits are phased to produce an along track separation of

$$B_{at} = a\sin(\nu_2)\,, \tag{6}$$

where ν_2 is the initial true anomaly of SC_2, and it is assumed that the initial true anomaly of SC_1 is $\nu_1 = 0$. For a pendulum PRO, both B_{at} and B_c must

Examples of the PROs are shown in the LVLH frame of SC_1 in Figure 1. The curves represent the motion of SC_2 relative to SC_1. The relative motion in a frozen corkscrew differs from that in a regular corkscrew by less than a millimeter, and so the frozen corkscrew is not shown in Figure 1. Consider the cartwheel PRO, shown as a dashed line with circles. It is in the orbital plane of SC_1 and can be approximated by the standard, 2×1 elliptical "football" orbit of the Hill-Clohessy-Wiltshire (HCW) Equations. Note, however, that the cartwheel is designed in the nonlinear, Keplerian orbital dynamics model and not a simplified, linearized model. The pendulum PRO is the approximately vertical line with asterisks (there are centimeter-level oscillations in the x- and y-directions). The pendulum can be approximated by a pure z-oscillation in the HCW Equations. The true anomaly offset in this case results in a 100 m y-offset. Finally, the corkscrew can be approximated as a football orbit combined with the z-oscillation of a pendulum.

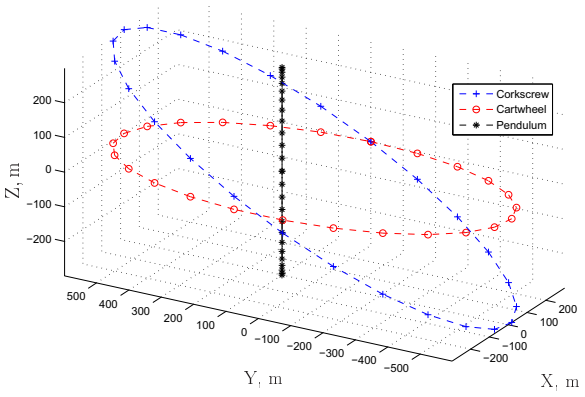

Figure 1. PROs Considered in InSAR Study

These InSAR PROs are based on Keplerian orbits, that is, based on the absolute motion of the two spacecraft. For formation control, we require a description of the relative spacecraft motion in a Cartesian LVLH frame. We parameterize the relative motion with a Fourier-like sum of sinusoidal basis functions, where the longest period is the orbital period of SC_1. Specifically, the parameterization is

$$\boldsymbol{x}_f(\nu_1) = \begin{bmatrix} \boldsymbol{\rho}_f(\nu_1) \\ \frac{d}{d\nu_1}\boldsymbol{\rho}_f(\nu_1) \end{bmatrix} = \begin{bmatrix} a_{10} + \sum_{k=1}^{N_p} \left(a_{1\,ck}\cos(k\nu_1) + a_{1\,sk}\sin(k\nu_1) \right) \\ a_{20} + \sum_{k=1}^{N_p} \left(a_{2ck}\cos(k\nu_1) + a_{2sk}\sin(k\nu_1) \right) \\ \vdots \\ a_{60} + \sum_{k=1}^{N_p} \left(a_{6ck}\cos(k\nu_1) + a_{6\,sk}\sin(k\nu_1) \right) \end{bmatrix}, \tag{7}$$

where $\boldsymbol{x}_f = [\,\boldsymbol{\rho}_f^T \;\; (d\boldsymbol{\rho}_f/d\nu_1)^T\,]^T$ is the fitted dynamic state vector of SC_2 with respect to SC_1 represented in the LVLH frame, ν_1 is the true anomaly of SC_1, $\boldsymbol{\rho}_f$ is the fitted relative position vector, a_{ick} and a_{isk} are constant coefficients, and N_p is the order of the basis function parameterization. Since $\boldsymbol{\rho}_f$ is a vector in the LVLH frame, its derivative is with respect to the LVLH frame.

In the formation guidance algorithm, the parameterization Eq. (7) is fit automatically. The specified Keplerian PRO is calculated for one orbital period, and the relative position and velocity of SC_2 in the LVLH frame is stored at discrete points. Then, for a given N_p, the coefficients $a_{1\,ck}$, a_{1sk}, a_{2ck}, etc. are solved for via least squares. The value for N_p is increased until the least squares residual is below a specified tolerance. Typically, $N_p = 3$ is sufficient to fit relative position to better than $1e$-7 m and relative velocity to better than $1e$-9 m/s for 2000 discrete points.

III. Formation Control Architecture and Algorithms

The Leader/Follower formation control architecture[8] was selected for this study since it is robust and its stability properties are well understood.[14] The Leader/Follower architecture is characterized by a hierarchical state dependency in spacecraft control laws. In contrast, Cyclic control architectures have a non-hierarchial control dependency. Even though Cyclic architectures can be more efficient, their stability is only understood in restricted cases.[24]

Based on the Leader/Follower controller architecture, a control algorithm must be designed for SC_2 to control itself relative to SC_1. To limit the scope of this study, the formation control algorithm is designed using the steady-state Linear Quadratic Regulator (LQR). The control design model is a version of the HCW Equations augmented with the effects of J_2.[25] The cross-track effects of J_2 are nonlinear and so we only retain the in-orbit-plane (i.e., the radial/along-track plane) terms.

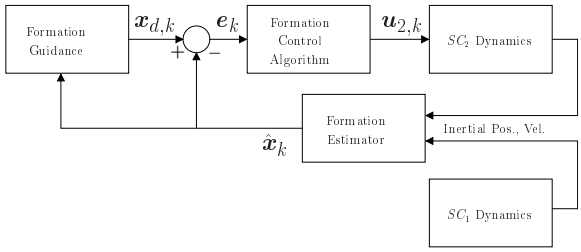

Figure 2. Two-Spacecraft Leader/Follower Control Architecture

As a brief review, the components of an overall formation guidance and control system specialized to our scenario are shown in Figure 2. We consider a discrete time formulation as would be implemented onboard a spacecraft. Assume the spacecraft computer has a control cycle of length T_s that starts at discrete times indexed by k (i.e., $T_s = t_{k+1} - t_k$). Each time step, the formation guidance generates a desired position and velocity $\boldsymbol{x}_{d,k} = [\;\boldsymbol{\rho}_{d,k}^T \;, \dot{\boldsymbol{\rho}}_{d,k}^T\;]^T$ of SC_2 with respect to SC_1 in the LVLH frame, where the $(\dot{})$ indicates differentiation with respect to time. The estimated relative state vector $\hat{\boldsymbol{x}}_k$ is subtracted from the desired relative state to obtain the control tracking error $\boldsymbol{e}_k$. The control error is then passed to the Leader/Follower formation control algorithm that generates the relative acceleration command $\boldsymbol{u}_{2,k}$, where $\boldsymbol{u}_{i,k}$ is the control acceleration for SC_i in the k^{th} time step.

For LQR design, the J_2-augmented HCW Equations must be discretized. Ignoring disturbances, the discretized equations of motion have the following form:

$$\boldsymbol{x}_{k+1} = A\boldsymbol{x}_k + B\boldsymbol{u}_k \tag{8}$$

where A and B are appropriately-sized matrices, the state vector $\boldsymbol{x}_k$ consists of relative position and velocity of SC_2 with respect to SC_1 in the LVLH frame of SC_1, and $\boldsymbol{u}_k = \boldsymbol{u}_{2,k}$. Recall $\boldsymbol{u}_{1,k}$ is uniformly zero, except for orbit maintenance and possibly reconfiguration maneuvers.

Two important aspects of the discretization process are (i) selecting the discrete time step size T_s, also referred to as the control sample period, and (ii) specifying how the control acceleration is applied in continuous time. Regarding the latter, the standard assumption is that $\boldsymbol{u}_{2,k}$ is applied constantly from t_k to t_{k+1}. This assumption does not necessarily give the desired performance. Instead, we assume that $\boldsymbol{u}_{2,k}$ is applied constantly from t_k to $t_k + T_\sigma$, where $0 < T_\sigma \leq T_s$. Both T_s and T_σ are control design parameters and affect A and B in Eq. (8).

The LQR controller is optimal in that it minimizes the cost

$$J = \sum_{k=0}^{\infty} \left(x_k^T Q x_k + u_k^T R\, u_k \right) \tag{9}$$

subject to Eq. (8), where $Q \geq 0$ and $R > 0$ are weighting matrices. The steady-state LQR controller[26] is given by $u_k = -Gx_k$ where $G = (B^T S B + R)^{-1} B^T S A$, and S is the solution to the algebraic Riccati equation

$$S = A^T [S - SB(B^T S B + R)^{-1} B^T S] A + Q\,. \tag{10}$$

We assume R is the identity matrix and

$$Q = \begin{bmatrix} \lambda_x & 0 & \cdots & & & \\ 0 & \lambda_y & 0 & \cdots & & \\ \cdots & 0 & \lambda_z & 0 & \cdots & \\ & \cdots & 0 & \lambda_v\lambda_x & 0 & \cdots \\ & & \cdots & 0 & \lambda_v\lambda_y & 0 \\ & & & \cdots & 0 & \lambda_v\lambda_z \end{bmatrix}, \tag{11}$$

where λ_x, λ_y, and λ_z weight the effect of position errors by axis, and λ_v scales these position weights to velocity weights. Each of the four weights is a design parameter.

The LQR controller is a regulator, that is, it is the optimal controller for driving the state to the origin of phase space. However, we wish the state trajectory to track a PRO. To formulate the optimal linear quadratic tracker (LQT), the LQR cost Eq. (9) is modified to

$$J_T = \sum_{k=0}^{\infty} (x_k - x_{d,k})^T Q (x_k - x_{d,k}) + u_k^T R\, u_k\,. \tag{12}$$

In the special case when $x_{d,k}$ is a homogenous solution of Eq. (8), that is, when $x_{d,k+1} = A_d x_{d,k}$, the LQT controller reduces to the LQR controller.[26] While not all the Keplerian PROs are not exact solutions to linearized models, and hence the LQR controller is sub-optimal, its performance is sufficient.

IV. Formation Guidance Algorithms

A formation guidance algorithm determines $\boldsymbol{x}_{d,k} = [\, \boldsymbol{\rho}_{d,k}^T \,, \dot{\boldsymbol{\rho}}_{d,k}^T \,]^T$, the desired relative position and velocity for SC_2. The Command Virtual Structure (CVS) guidance architecture developed here is an adaptation of a common Cyclic combined guidance/control architecture called Iterated Virtual Structure (IVS).[27,28] In IVS, a formation template or "virtual structure" is fit to the spacecraft positions at the beginning of each time step. Then the spacecraft control to their fitted positions for that time step. The stability of an IVS control design is inferred from simulation. Aspects of IVS have been incorporated in other Cyclic algorithms, such as centroiding approaches, where the location but not the orientation of the template is fit.[18] Here, IVS is modified to obtain a Leader/Follower-compliant guidance algorithm by fitting only the orientation of the formation template.

This study considers two formation guidance algorithms: CVS and Prescribed-ν Guidance. The latter may be considered the standard Leader/Follower approach. Prescribed-ν guidance commands SC_2 to track the exact PRO in both time and space via

$$\boldsymbol{\rho}_{d,k} = \boldsymbol{\rho}_f(\hat{\theta}_{1,k} - n2\pi) \tag{13a}$$

$$\dot{\boldsymbol{\rho}}_{d,k} = \widehat{\frac{d\nu_1}{dt}} \left[\frac{d}{d\nu_1} \boldsymbol{\rho}_f(\nu_1) \right] \Bigg|_{\nu_1 = \widehat{\theta}_{1,k} - n2\pi} \tag{13b}$$

where $\widehat{\theta}_{1,k}$ is the estimated argument of latitude of SC_1 at time step k, n is the largest integer such that $n2\pi \leq \hat{\theta}_{1,k}$, and the estimated true anomaly rate is given by

$$\widehat{\frac{d\nu_1}{dt}} = \frac{1}{\|\hat{\boldsymbol{r}}_{1,k}\|^2} \|\hat{\boldsymbol{r}}_{1,k} \times \hat{\boldsymbol{v}}_{1,k}\|, \qquad (14)$$

where $\hat{\boldsymbol{r}}_{1,k}$ and $\hat{\boldsymbol{v}}_{1,k}$ are the estimated position and velocity of SC_1 in an Earth-centered, reference frame at time step k. Such information would be available from GPS. In the arguments of $\boldsymbol{\rho}_f$ in Eq. (13), the true anomaly of SC_1 has been replaced with the estimated argument of latitude. This substitution is necessary to account for the J_2-induced perturbation of the argument of perigee of SC_1. See Figure 3, which illustrates the need for the argument of latitude.

The CVS guidance algorithm (conceived by E.A. Murray) is based on the observation that the time history of the relative motion can vary temporally as long as the commanded relative motion follows the PRO path spatially. Hence, we set the desired relative position at t_k to

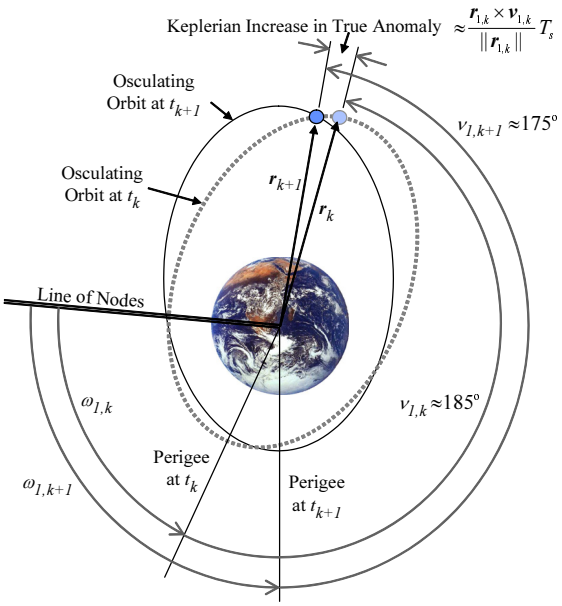

Figure 3. Illustration of Periapsis Motion that Necessitates Use of Argument of Latitude in Formation Guidance. In this exaggerated example, the true anomaly decreases as time increases from t_k to t_{k+1}. However, the argument of latitude $\theta_1 = \omega_1 + \nu_1$ increases by approximately the Keplerian value.

$$\boldsymbol{\rho}_{d,k} = \boldsymbol{\rho}_f\Big(\alpha_k[\,\hat{\theta}_{1,k} - n2\pi]\Big) \qquad (15a)$$

$$\dot{\boldsymbol{\rho}}_{d,k} = \widehat{\frac{d\nu_1}{dt}} \left[\frac{d}{d\nu_1}\boldsymbol{\rho}_f(\nu_1)\right]\Big|_{\nu_1 = \alpha_k[\,\hat{\theta}_{1,k} - n2\pi]} \qquad (15b)$$

for some time-varying α_k that we select. If $\alpha_k = 1$ uniformly, then Eq. (15) reduces to Prescribed-ν Guidance. To maintain phasing between InSAR baselines and orbital position, it is further desired that $1-\delta \leq \alpha_k \leq 1+\delta$ for some small δ.

The extra degree of freedom introduced by α_k is used to reduce Δv requirements. Specifically, the formation guidance algorithm calculates the minimum weighted tracking error e_k^* via

$$\boldsymbol{e}_k^* = \min_{\tau \in [\,0,\,2\pi\,]} \left\| \begin{bmatrix} \hat{\boldsymbol{\rho}}_k \\ \gamma \widehat{\frac{dt}{d\nu_1}} \hat{\dot{\boldsymbol{\rho}}}_k \end{bmatrix} - \begin{bmatrix} \boldsymbol{\rho}_f(\tau) \\ \gamma \frac{d}{d\nu_1}\boldsymbol{\rho}_f(\tau) \end{bmatrix} \right\|, \qquad (16)$$

where the estimated inverse true anomaly rate $\widehat{dt/d\nu_1}$ is obtained from Eq. (14), $\hat{\boldsymbol{\rho}}_k$ and $\hat{\dot{\boldsymbol{\rho}}}_k$ are the estimated relative position and velocity of SC_2 in the LVLH frame, and γ is a velocity error weight. This weight is a design parameter, and should be tuned in concert with λ_v. The parameter α_k is solved for implicity in Eq. (16).

The minimization in Eq. (16) can have multiple minima. We solve this problem by discretizing the interval $[\,0,\,2\pi\,]$ and applying exhaustive search. Then a local optimization is performed with the minimum point as an initial condition.

Figure 4 illustrates the two guidance approaches and the difference between them for $\gamma = 0$. An example PRO is shown in the LVLH frame of SC_1, which is at the center of the ellipse. SC_2 travels along the elliptical PRO, and several time steps are indicated by values of ν_1. These are the positions SC_2 would assume if there were no disturbances. However, with disturbances and without control SC_2 follows the

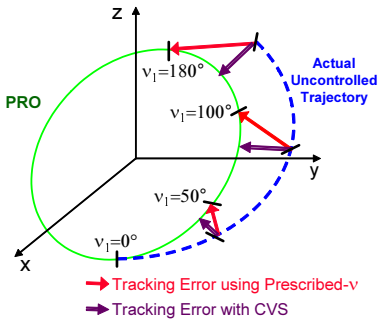

Figure 4. Prescribed-ν and CVS Guidance

dashed line with the corresponding steps of ν_1 shown. For Prescribed-ν Guidance, the tracking error is the difference between the dashed and solid lines at the time steps as shown by solid arrows. For CVS with $\gamma = 0$, the tracking error is the minimum distance to the PRO.

V. Simulation Environment and Assumptions

A MATLAB-based formation flying simulation environment was developed to evaluate the two-spacecraft formation flying scenarios. The dynamics include forces due to a radially symmetric Earth and Earth oblateness as characterized by the first four zonal harmonics J_2 through J_6. The dynamics also model aerodynamic drag. However, to evaluate Δv requirements for maintaining PROs, sometimes several hundred orbits had to be averaged over. Since drag decreases the semi-major axes and the orbit maintenance/reconfiguration algorithm has not yet been fully integrated into the simulation environment, drag was omitted. As discussed in the Introduction, differential aerodynamic drag is three orders-of-magnitude smaller than differential J_2.

The simulation environment uses a fixed-step, 5^{th} order Runge-Khutta integrator. The integrator time step was $1/100^{th}$ of SC_1's initial orbit (1 minute). Simulations were also performed with a time step 10 times smaller with no appreciable difference. The initial inclination for SC_1 was always 97.4°. The control sample period T_s wass $1/100^{th}$ of SC_1's initial Keplerian orbit, and the control actuation time T_σ was 1 s. These effects of varying these two control parameters are analyzed in the next section.

For sensor noise levels, we used carrier differential GPS (CDGPS) results from two- and three-spacecraft ground-based formation estimation testbeds,[29–31] which have achieved relative sensing of $2\,cm$ and $0.5\,mm/s$ 1σ in relative position and velocity. For absolute knowledge, we assume GPS has real-time sensor noise of $1\,m$ 1σ.[32,33] With accelerometers in addition to GPS, it was assumed absolute velocity knowledge was accurate to 0.1 m/s 1σ. These values are mildly conservative since with the global differential correction system, real-time GPS position uncertainty can be reduced to tens of centimeters.[34] Actuator uncertainties included a thrust magnitude variation uniformly distributed in ±5% of the requested value, attitude uncertainty of 1 $arcmin$ (for transforming LVLH requested forces to body frame for thrust allocation), and thruster misalignments of 15 $arcsec$.

However, sensor noise and actuation uncertainties were not included in the simulations for Δv and acceleration requirements. Differences in Δv requirements between these cases and their corresponding cases without sensor and actuator uncertainties are less than 1.5%. Sensor noise and actuator uncertainties were included in the controller parameter sensitivity study since as the sample period T_s gets larger, sensor noise can become the principal limitation achievable tracking performance.[16]

VI. InSAR Δv Requirements

To determine formation Δv requirements, a spectrum of PRO classes, orbit altitudes, baselines, and controller error requirements were considered. The error requirements are specified as (e_x, e_y, e_z), where e_i is the tracking error allowed in a given LVLH axis. For example, if e_z is $10\,m$, then the difference between the commanded z relative position and the actual can be $\pm 10\,m$. Generally, the e_y requirement is larger than those for e_x and e_z since the InSAR formation is less sensitive to baseline offsets in the along-track direction. Table 1 shows the values considered in this study.

PRO Class	Orbit Altitude(km)/ InSAR Baseline(m)	Performance Requirements (m)
Corkscrew, $\omega_1 = 0°$ and 90°	500/300	(10,50,10)
Pseudo-Frozen Corkscrew	500/1000	(25,125,25)
Cartwheel $\omega_1 = 0°$ and 90°	1000/2000	(50,250,50)
Pendulum $\omega_1 = 0°$ and 90°		

Table 1. Characteristics of InSAR Formations to be Studied

Figures 5 and 6 show representative Δv requirements and tracking errors for formation control using CVS for a 500 km corkscrew with 90° initial argument of perigee and 300 m baselines. Additionally, Figure 5 shows the Δv requirement for controlling the same PRO using Prescribed-ν formation guidance. The Δv requirements are shown as the average Δv required per orbit up to a given time. For example, the average

Δv per orbit at 1000 orbits in Figure 5 is the total Δv required over those 1000 orbits divided by 1000. For this PRO, CVS reduces the required Δv by 16%.

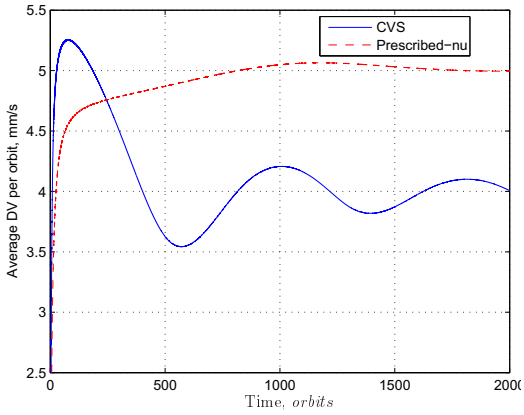

Figure 5. Δv Requirements for a Corkscrew PRO with $500km$ Altitude, 90° Initial Perigee, and $300m$ Baseline for Both Prescribed-ν and CVS Formation Guidance.

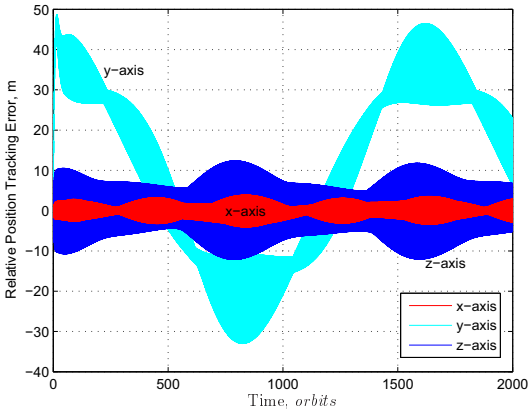

Figure 6. Tracking Error for a Corkscrew PRO with CVS, $500km$ Altitude, $300m$ Baseline, and $(10, 25, 10)m$ Error Requirements

The Δv requirements for the test cases of Table 1 using CVS formation guidance are shown in Table 2. The Δv requirements using Prescribed-ν are still being determined, and initial results are shown in Table 3. The values for "w" are the initial argument of perigee.

These results show that operating a distributed InSAR mission as a formation is feasible: the majority of Δv requirements are less than $12\,mm/s/orbit$. Figure 7 can be used to interpret these Δv requirements. The figure shows the percentage of initial spacecraft wet mass that is fuel for a two-year mission with a semi-major axis of $7128\,km$ ($750\,m$ altitude) as a function of average Δv per orbit for both cold gas thrusters (I_{sp} of $60\,s$) and electric thrusters (I_{sp} of $2500\,s$). For $12\,mm/s/orbit$, the fuel mass percentages are 18% and 0.3% for cold gas and electric thrusters, respectively.

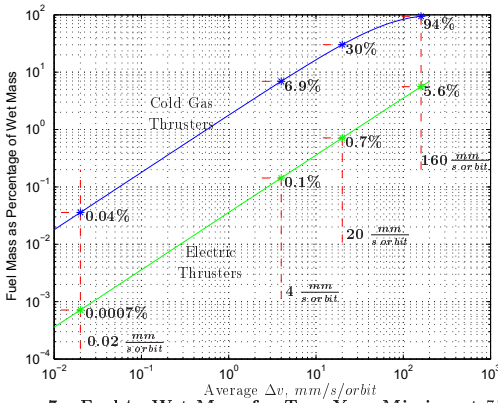

Figure 7. Fuel-to-Wet-Mass for Two Year Mission at $750\,km$ Altitude

VI.A. Comparison of Prescribed-ν and CVS Guidance

Figure 5 shows one comparison between the Δv required by a formation using CVS and a formation using Prescribed-ν guidance algorithms. Considering Tables 2 and 3, CVS requires less Δv for cartwheel and pendulum PROs and for corkscrews with 90° initial perigee. Figure 8 shows a case where CVS uses 89% less Δv, that is, nearly an order of magnitude improvement.

CVS achieves these savings by introducing a bias into the rate at which SC_2 travels around the PRO. Figure 9 shows the difference between the CVS command for the angular position of SC_2 in a corkscrew PRO and the the true anomaly of SC_1, ν_1. For Prescribed-ν, this difference is uniformly zero. When this difference reaches, for example, 90°, then a baseline that originally occurred at the equator now occurs at one of the poles. This secular drift, which is on the order of tenths of a degree per orbit, can be desirable for shifting baselines. If, however, the time at which a baseline occurs is to remain fixed, then the secular drift must be restricted. Also shown in Figure 9 is a version of constrained CVS in which the difference between the CVS command and ν_1 is limited to 10°. As can be seen from the figure, after several days, constrained CVS is equivalent to Prescribed-ν with a constant offset.

Orbit altitude/Baseline 500 km/300 m		Desired Error Box		
		10/50/10	25/125/25	50/250/50
Orbit Type	Corkscrew, w = 0, CVS	3.99	3.84	3.83
	Corkscrew, w = 90, CVS	4.42	3.84	3.78
	Pseudo-frozen corkscrew, CVS	4.17	3.82	3.90
	Cartwheel, w = 0, CVS	0.95	0.45	0.02
	Cartwheel, w = 90, CVS	0.12	0.06	0.06
	Pendulum, CVS	1.89	0.64	0.73
Orbit altitude/Baseline 500 km/1000 m		**Desired Error Box**		
				50/250/50
Orbit Type	Corkscrew, w = 0, CVS			12.78
	Corkscrew, w = 90, CVS			12.84
	Pseudo-frozen corkscrew, CVS			12.90
	Cartwheel, w = 0, CVS			0.24
	Cartwheel, w = 90, CVS			0.26
	Pendulum, CVS			2.09
Orbit altitude/Baseline 1000 km/2000 m		**Desired Error Box**		
		10/50/10		50/250/50
Orbit Type	Corkscrew, w = 0, CVS	70.50		21.50
	Corkscrew, w = 90, CVS	160.50		25.55
	Pseudo-frozen corkscrew, CVS	33.40		20.90
	Cartwheel, w = 0, CVS	10.60		1.43
	Cartwheel, w = 90, CVS	13.60		0.97
	Pendulum, CVS	5.83		3.60

Table 2. InSAR Formation Study Average Δv per Orbit, $mm/s/orbit$ for CVS Formation Guidance

Orbit altitude/Baseline 500 km/300 m		Desired Error Box		
		10/50/10	25/125/25	50/250/50
Orbit Type	Corkscrew, w = 0, Pnu	4.76	4.68	4.63
	Corkscrew, w = 90, Pnu	1.06	1.02	0.98
	Pseudo-frozen corkscrew, Pnu	1.05	1.02	0.99
	Cartwheel, w = 0, Pnu	1.06	1.02	0.99
	Cartwheel, w = 90, Pnu	1.18	1.02	0.99
	Pendulum, w=0 Pnu	3.71	3.69	3.67
	Pendulum, w=90 Pnu	0.00	0.00	0.00

Table 3. InSAR Formation Study Average Δv per Orbit, $mm/s/orbit$ for Prescribed-ν Formation Guidance

VI.B. Acceleration Requirements

In addition to Δv requirements, a formation control system must have realizable acceleration requirements. The force level of RCS thrusters can range from Newtons for cold gas to milli- and micro-Newtons for electric thrusters. For a $1000\,kg$ spacecraft, this translates into acceleration levels of mm/s^2 to nm/s^2. A large ion thruster, such as the UK-25, can produce $300\,mN$ of thrust. Figure 10 shows the maximum acceleration for each of the CVS test cases and the acceleration limit for a large ion thruster. These acceleration levels are easily realizable with a cold gas RCS system, but are large for an electric thruster RCS system using $3-30\,mN$ electric thrusters.

Recall that the CVS test cases used control design parameters $T_s = 1/100^{th}$ of an orbit and $T_\sigma = 1.0\,s$. T_s is the control sample period, and T_σ is the duration that a commanded acceleration level is applied. A sensitivity analysis was performed to determine the impact of varying these parameters on formation Δv

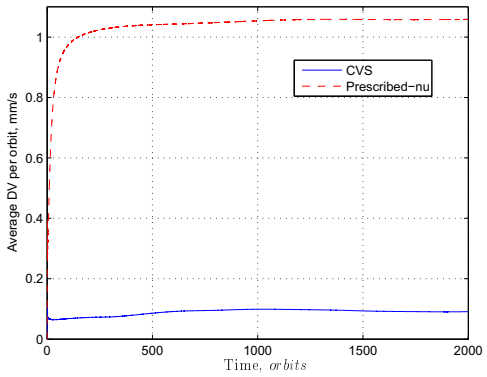

Figure 8. Δv Requirements for a Cartwheel PRO with $500km$ Altitude, 90° Initial Perigee, and $300m$ Baseline for Both Prescribed-ν and CVS Formation Guidance.

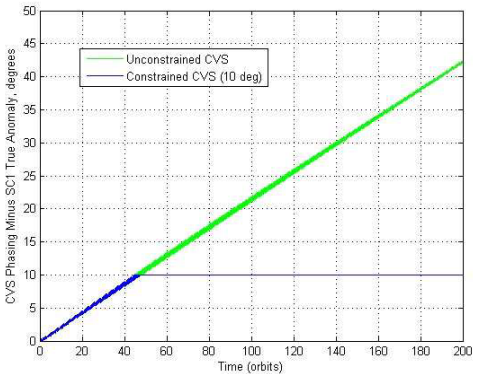

Figure 9. Difference Between Formation Guidance Command and ν_1 for CVS and Constrained-CVS. For Prescribed-ν, this difference is uniformly zero.

and acceleration requirements.

Tables 4 and 5 show the results for a corkscrew PRO using CVS with $10/50/10\,m$ tracking error requirements. In these tables, the non-dimensional parameter $\sigma = T_\sigma/T_s$ replaces T_σ. If $\sigma = 1$, then SC_2 is always thrusting. From Table 4 we first conclude that the non-dimensionalized sample period, T_s/orbit period, and σ can be varied from nearly zero to nearly one with minimal impact on the Δv requirement. Furthermore, the longest control sample period that does not significantly affect Δv is $1/3^{rd}$ of an orbit. This period compares favorably with some model predictive control approaches that thrust every half orbit.[16] Next, from Table 5 it is seen that for a $1000\,kg$ spacecraft with constant thrusting, standard, milli-Newton-level electric thrusters can be used. If desired, thrusting could be done only half the time ($\sigma = 0.5$) and still only require micro-Newton-level accelerations.

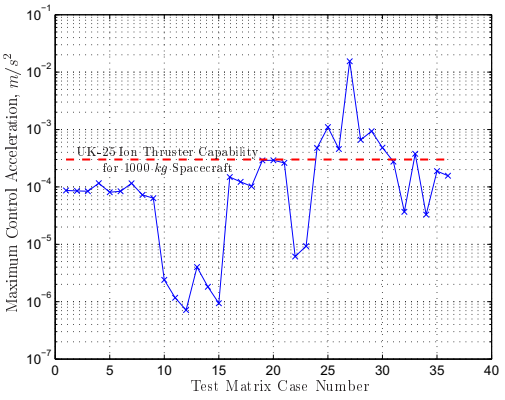

Figure 10. Maximum Control Accelerations

Fraction of Orbit Period Ts	σ 0.001	0.005	0.01	0.05	0.1	0.5	1
1/100	4.74	4.74	4.74	4.74	4.74	4.73	4.73
1/50	4.74	4.74	4.74	4.74	4.74	4.73	4.73
1/10	4.74	4.74	4.74	4.74	4.74	4.74	4.77
1/5	4.74	4.73	4.73	4.73	4.73	4.77	5.01
1/3	4.92	4.95	4.94	4.96	4.96	5.21	5.84

Table 4. Δv Requirements in m/s for a Cartwheel PRO with $500\,km$ Altitude, 90° Initial Perigee, $300\,m$ Baseline, and CVS Formation Guidance as a Function of Control Design Parameters.

Fraction of Orbit Period Ts	σ 0.001	0.005	0.01	0.05	0.1	0.5	1
1/100	1.4E-03	2.8E-04	1.4E-04	2.8E-05	1.4E-05	2.8E-06	1.4E-06
1/50	1.4E-03	2.8E-04	1.4E-04	2.8E-05	1.4E-05	2.8E-06	1.4E-06
1/10	1.3E-03	2.8E-04	1.4E-04	2.7E-05	1.4E-05	2.8E-06	1.4E-06
1/5	1.3E-03	2.7E-04	1.3E-04	2.7E-05	1.3E-05	2.8E-06	1.5E-06
1/3	1.4E-03	3.0E-04	1.4E-04	2.8E-05	1.4E-05	3.2E-06	1.7E-06

Table 5. Acceleration Requirements in m/s^2 for a Cartwheel PRO with $500\,km$ Altitude, 90° Initial Perigee, $300\,m$ Baseline, and CVS Formation Guidance as a Function of Control Design Parameters.

Having discussed formation guidance and control issues for maintaining a PRO, we now turn to formation algorithms for maintaining the absolute formation orbit and changing PROs.

VII. Orbit Maintenance/Reconfiguration Algorithm

VII.A. Problem Statement

The goal of the formation guidance OM/R algorithm is to plan fuel-optimal, acceleration-limited trajectories that maneuver two spacecraft in LEO from arbitrary initial conditions to final conditions specified by (i) the desired absolute orbit of the formation, and (ii) the desired PRO of SC_2 with respect to SC_1. This trajectory planning problem is a complex, nonlinear optimization problem that remains unsolved in its general form. Consistent with the scope of this study, we have made simplifying assumptions to obtain a near-optimal, computationally-efficient algorithm for evaluating formation fuel consumption. These assumptions are discussed subsequently.

Figure 11 shows the problem statement graphically. Let $X(0)$ be the initial position on the desired formation reference orbit with respect to Earth's center. This reference orbit is independent of the spacecraft states, has initial true anomaly $\nu(0)$, and defines an LVLH frame. Subsequently, we allow $\nu(0)$ to vary. The initial positions of SC_1 and SC_2 relative to the formation reference orbit in the LVLH frame are given by $\boldsymbol{\rho}_1(0)$ and $\boldsymbol{\rho}_2(0)$, respectively. The final condition of the formation reconfiguration or orbit maintenance maneuver consists of (i) SC_1 located on the formation reference orbit and (ii) SC_2 in the desired PRO.

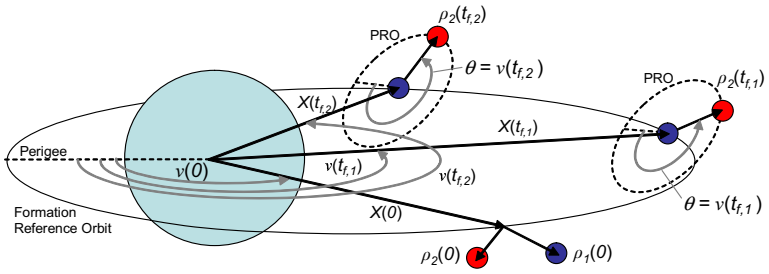

Figure 11. OM/R Problem Statement

A key aspect of this problem is that the maneuver time is free. That is, as long as the maneuver is completed in some reasonable maximum amount of time, it can take half an orbit or three orbits. Figure 11 shows the final conditions for two different maneuver times, $t_{f,1}$ and $t_{f,2}$. Observe that the final PRO has the same shape for both maneuver times, but that the location of SC_2 within the PRO depends on the maneuver time. Another key aspect is that SAR spacecraft may not have a large "kick" motor for impulsive velocity changes. Hence, the OM/R algorithm must include the ability to plan low-thrust optimal trajectories. For example, assuming 5 N cold-gas thrusters are mounted on a 1000 kg spacecraft and two thrusters must fire to produce a pure force, translational accelerations are limited to 0.01 m/s^2.

VII.B. OM/R Algorithm Assumptions

To obtain a computationally-efficient, practical algorithm, we make the following assumptions. First, there are no environmental disturbances (i.e., no drag, solar pressure, or gravitational perturbations). The OM/R algorithm does partially account for J_2. However, for simplicity, we present the disturbance-free case. Second, each spacecraft has six thrusters that point in each of the cardinal directions of the LVLH frame. Each thruster can produce a maximum acceleration of u_{max}. Third, we are currently not considering collision avoidance. Our experience is that the planned trajectories of the two spacecraft rarely intersect. However, in future versions of this algorithm, collision avoidance can be included through either waypoints or starting the spacecraft along their trajectories at different times. See Ref. 35 for more on collision avoidance through phasing of maneuver start times. Finally, the spacecraft remain close enough to the formation reference orbit that linearized relative dynamics are accurate (i.e., tens of kilometers). If this last assumption is violated, the OM/R algorithm will still function, but it will be sub-optimal.

For orbit maintenance, the initial relative positions of the two spacecraft are close to the desired PRO, but the spacecraft have drifted away from their absolute formation orbit. The OM/R algorithm returns SC_1 to the origin of the LVLH frame and SC_2 to the desired PRO about SC_1.

A reconfiguration maneuver changes the PRO of SC_2 about SC_1. Since SC_1's orbit is already close to the desired absolute orbit, only SC_2 maneuvers. To balance fuel consumption, a reconfiguration can also be used to switch the roles of SC_1 and SC_2.

VII.C. OM/R Solution

Our solution method is to apply linear programming to the HCW Equations augmented with the in-orbit-plane effects of J_2.[25] The eccentricities of the orbits for which the OM/R algorithm will be used are very small (10^{-5}), and so the HCW Equations are a valid approximation. Further, eccentricities of up to 0.2 can be included without restructuring the OM/R algorithm via time-explicit, eccentricity series-based linear relative dynamic models.[36] The application of linear programming to relative path planning of spacecraft is not new.[9,37] Our contributions are to generalize the boundary conditions and introduce an additional degree of freedom that further reduces fuel consumption.

Given a discrete, linear, time-invariant model of the form of Eq. (8), the state at time step k can be written in terms of initial conditions x_0 (e.g., $\boldsymbol{\rho}_2(0)$ and the associated velocity in Figure 11) and all previous thruster firings u_i, $i = 0, \ldots, k-1$ as

$$x_k = G_k U_k + c_k \tag{17a}$$

$$G_k = [\, A^{k-1}B \; A^{k-2}B \; \cdots \; AB \; B \,] \tag{17b}$$

$$c_k = B^k x_0 \tag{17c}$$

$$U_k = [\, u_0^T \; u_1^T \; \cdots \; u_{k-1}^T \,]^T \tag{17d}$$

The trajectory optimization problem can now be formulated as a linear program. The goal is to have x_n equal the desired final conditions x_f while minimizing the fuel consumed. The fuel consumed is monotonically related to sum of the absolute values of the thruster accelerations. Finally, recall that the thrust must be

limited to u_{max}. The trajectory optimization problem can be stated in standardized form as

$$\min_{\Lambda_n} [\,1 \cdots 1\,]\Lambda_n$$
$$\text{subject to} \begin{cases} [\,G_n \;\; -G_n\,]\Lambda_n = x_f - c_n \\ \begin{bmatrix} I \\ -I \end{bmatrix} \Lambda_n \le \begin{bmatrix} u_{max} \\ 0 \end{bmatrix} \\ \Lambda_n = \begin{bmatrix} \Lambda_n^+ \\ \Lambda_n^- \end{bmatrix} \end{cases} \tag{18}$$

where $U_n = \Lambda_n^+ - \Lambda_n^-$. Since both Λ_n^+ and Λ_n^- are constrained to be positive, if $u_k = -1\ m/s^2$ for example, then the corresponding entry in Λ_n^+ would be 0 and in Λ_n^- the entry would be 1. While entries 1 and 2 would generate the same u_k, these values are not minimal. Hence, minimizing the sum of the elements of Λ_n is equivalent to minimizing the sum of the absolute values of the thruster accelerations.

The orbit maintenance and reconfiguration problems have been reduced to a linear program for which standard numerical solution software exists. However, the OM/R algorithm must still optimize over the final time, which changes x_f. Further, we also optimize over the initial formation reference point $\nu(0)$, which changes the LVLH frame and hence x_0. The maneuver final time is optimized by considering several discrete values. For shorter final times and smaller values of u_{max}, the linear program becomes infeasible. This infeasibility indicates that the maneuver cannot be completed in the given time with the given acceleration limit.

To understand how the reference LVLH frame enters the optimization, observe that the trajectory optimization problem only requires a spacecraft state relative to an LVLH frame. The transformation of the inertial spacecraft states to LVLH-relative states introduces an additional degree of freedom to optimize over. Specifically, we are free to choose any LVLH frame on the formation reference orbit within given limits. Choosing different LVLH frames only affects the time of perigee passage for the final formation orbit. Recall that Earth oblateness will be perturbing the time of perigee passage, and so modifying this time slightly during an orbit maintenance maneuver is not a concern. Further, it is shown subsequently that the optimum modifications are typically less than 0.05° in true anomaly.

Consider Figure 12. The default frame is the LVLH frame of the reference orbit of SC_1, which is point O_o in Figure 12. Recall this point is assumed to be within tens of kilometers of the spacecraft for the linearized dynamics to be accurate. The possible reference frames are parameterized by a true anomaly offset ν_{os} with respect to the default reference frame. For example, a second reference frame is shown with origin O_o'. When changing the reference LVLH frame, the specification of the final position of SC_2 within the desired PRO must account for ν_{os}. Therefore, the angle θ specifying the final position of SC_2 in the desired PRO is $\theta = \nu(0) + \nu_{os} + \Delta\nu_{mt}$, where $\Delta\nu_{mt}$ is the change in true anomaly over the maneuver time t_f.

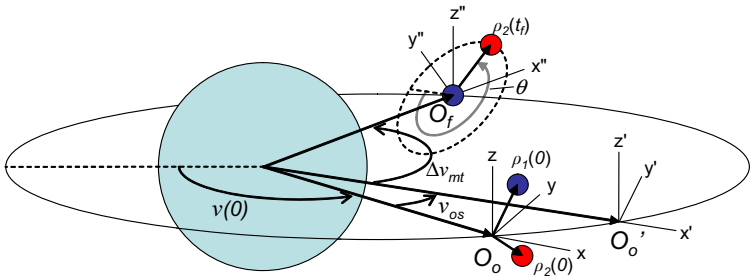

Figure 12. Varying the LVLH Reference Frame for Optimization

In summary, the OM/R algorithm considers ranges of maneuver times t_f and LVLH reference frame offsets ν_{os}. For each combination of maneuver time and offset, the trajectory optimization linear program of Eq. (18) is solved. From the resulting family of trajectories, the overall fuel optimal is selected.

VII.D. OM/R Algorithm Validation and Performance

The OM/R algorithm was verified by comparing to it a Hohmann transfer from a 499 km circular orbit to a 500 km circular orbit. To represent an impulsive transfer, u_{max} was set to 1 m/s^2. The Hohmann transfer time is 0.4995 of the period of the higher orbit, P_1. The default LVLH frame frame corresponded to the point in the higher orbit directly above SC_1's initial location on the lower orbit. Optimization over ν_{os} was performed. The resultant optimal ν_{os} was 0.03°. This offset is precisely the one needed so that the LVLH

frame, to which SC_1 is moving, ends at the correct point on the higher orbit. That is, with $\nu(0) = 0°$, $\nu_{os} = 0.03°$, and $t_f = 0.4995P_1$, we have $\nu(t_f) = 180°$ as is required for a Hohmann transfer. See Figure 13. The Hohmann Δv is $0.553\ m/s$ and the OM/R algorithm calculated a trajectory with a Δv of $0.555\ m/s$, that is, with 0.3% higher Δv. The Hohmann transfer and the impulsive OM/R transfer are shown in the reference LVLH frame in Figure 14.

Of more interest is how the OM/R algorithm performs with limited acceleration. Assume $u_{max} = 0.01\ m/s^2$, corresponding to an orbit transfer on RCS thrusters. The maneuver time is free. The OM/R algorithm calculated a trajectory taking 0.75 orbits, but with a Δv only 0.1% greater than the globally optimal Hohmann Δv. This lower-thrust trajectory is also shown in Figure 14. The optimal ν_{os} is 0.02°. Without optimizing over ν_{os} the sub-optimal trajectory required 6% more Δv. See Figure 15, which shows the optimal Δv as a function of ν_{os} for this lower-thrust case.

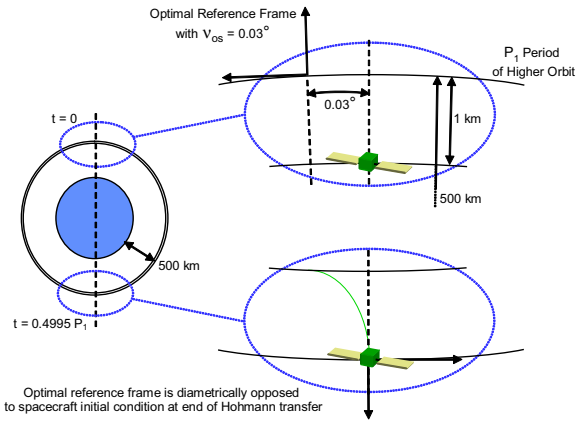

Figure 13. Hohmann Transfer Test Case for Verification of OM/R Algorithm

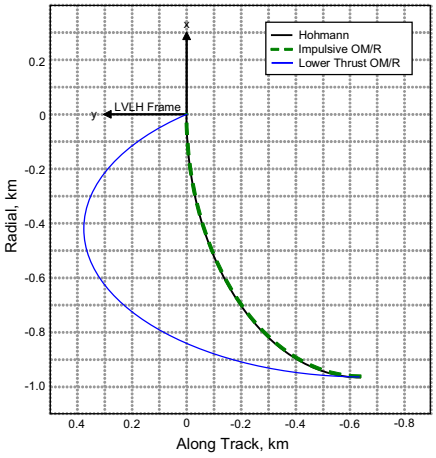

Figure 14. Hohmann, Impulsive-OM/R, and Lower Thrust-OM/R Trajectories in Reference LVLH Frames for $1\ km$ Transfer Between Circular Orbits. Note that the reference frame for the Lower Thrust-OM/R trajectory is different.

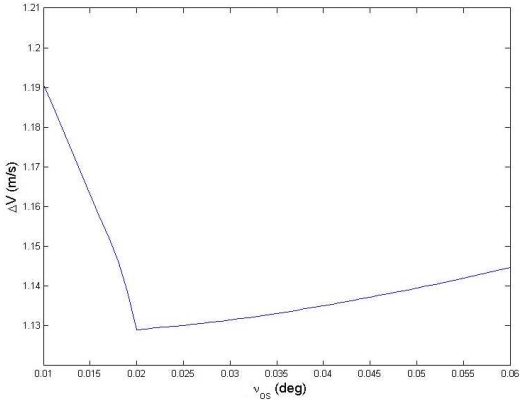

Figure 15. Optimal Δv for Lower Thrust-OM/R Trajectory as a Function of ν_{os}

The OM/R algorithm was used to determine representative Δv requirements for InSAR formation reconfigurations. Table 6 shows the Δv requirements for transferring between PROs at a representative altitude of $500\ km$ and baselines of $300\ m$. Reconfigurations can require from nearly $0.86\ m/s$ down to $0.16\ m/s$, which are equivalent to approximately 15 days and 2.8 days of formation control, respectively.

		Final PRO		
		corkscrew	cartwheel	pendulum
Initial PRO	corkscrew	--	0.3423	0.8301
	cartwheel	0.3423	--	0.6641
	pendulum	0.4984	0.1664	--

Table 6. Δv Requirements in m/s for Reconfigurations at $500\,km$ Altitude and $300\ m$ Baselines

VIII. Summary and Future Work

To evaluate the feasibility of formation flying two InSAR spacecraft, formation guidance, control, reconfiguration, and orbit maintenance architectures and algorithms have been developed, including the new CVS formation guidance algorithm. CVS incorporates some of the fuel-efficiency of Cyclic formation control schemes while maintaining the stability guarantees of the Leader/Follower architecture. It can reduce Δv requirements by up to an order of magnitude over standard Leader/Follower guidance schemes, such as Prescribed-ν. The principle underlying CVS is that baselines are allowed to vary temporally; the formation controls to the set of PRO baselines as opposed to a prescribed point in time and space. CVS achieves its Δv savings by introducing a secular drift in the phasing of a PRO. This drift can be used to shift phasing for InSAR observations.

Formation Δv and acceleration requirements were determined to maintain a spectrum of PROs. Generally, less than 12 $mm/s/orbit$ of Δv was required, resulting in fuel mass percentages of better than 18% for cold gas thrusters and 0.5% for electric thrusters. It was further determined that by varying control design parameters, the maximum acceleration required for formation maintenance can be tailored from $\mu m/s^2$ to mm/s^2. Hence, for a 1000 kg spacecraft, milli-Newton-level electric thrusters can be used for formation control.

Finally, an orbit maintenance/reconfiguration (OM/R) algorithm was developed for both maintaining the absolute formation orbit and reconfiguring between passive relative orbits for InSAR observations. A key aspect of this algorithm is that it includes acceleration magnitude constraints so that such maneuvers can be performed using RCS thrusters, obviating the need for a kick motor. To achieve optimal trajectories, it is critical to optimize over the LVLH frame in which the trajectory generation is performed. By doing so, a lower-thrust transfer was obtained that required the same Δv as an impulsive Hohmann transfer. Reconfigurations required Δv equivalent to a few days to a half-month of formation maintenance.

In our future work we intend to (i) incorporate OM/R algorithm into closed loop simulation environment and obtain mission Δv requirements with re-boosting, reconfigurations, oblateness, aerodynamic drag, solar radiation pressure, and sensor and actuator uncertainties, (ii) tailor the formation control laws to provide acceleration uncertainties on the order 10 nm/s^2 to allow for sub-millimeter precision orbit determination for radar data post-processing, and (iii) evaluate formation control with sensor noise levels corresponding to differential GPS as opposed to carrier differential GPS.

IX. Acknowledgments

This research was performed at the Jet Propulsion Laboratory, California Institute of Technology, under contract with the United States Air Force through the National Aeronautics and Space Administration. We thank the Aerospace Corporation for continuing technical and programmatic support of our efforts, particularly Dr. Nicholas Marechal and Dr. George Chao for fruitful technical exchanges.

References

[1]van Zyl, J., "The Shuttle Radar Topography Mission (SRTM): A Breakthrough in Remote Sensi ng of Topography," *Acta Astronautica*, Vol. 48, No. 5-12, 2001, pp. 559–565.

[2]Mellors, R., Magistrale, H., Earle, P., and Cogbill, A., "Comparison of four moderate-size earthquakes in southern California using seismology an InSAR," *Bulletin of the Seismological Society of America*, Vol. 94, No. 6, 2004, pp. 2004–2014.

[3]Forster, R., Jezek, K., Sohn, H., Gray, A., and Matter, K., "Analysis of glacier flow dynamics from preliminary RADARSAT InSAR data of the Antarctic mapping mission," *Intl. Geoscience and Remote Sensing Symposium (IGARSS)*, 1998, pp. 2225–2227.

[4]Kong, E., Miller, D., and Sedwick, R., "Exploiting Orbital Dynamics for Aperture Synthesis using Distributed Satellite Systems: Applications to a Visible Earth Imager System," *J. Astro. Sci.*, Vol. 47, No. 1, 1999, pp. 53–75.

[5]Fiedler, H. and Krieger, G., "Close Formation of Micro-Satellites for SAR Interferometry," *2nd Int. Symp. on Formation Flying Missions & Technologies*, Washington, DC, 2004.

[6]Scharf, D., Ploen, S., and Hadaegh, F., "A Survey of Spacecraft Formation Flying Guidance and Control (Part I): Guidance," *Amer. Contr. Conf.*, 2003.

[7]Gill, E. and Runge, H., "Tight formation flying for an along-track SAR interferometer," *Acta Astronautica*, Vol. 55, No. 3-9, 2004, pp. 473–485.

[8]Wang, P. and Hadaegh, F., "Coordination and Control of Multiple Microspacecraft Moving in Formation," *J. Astro. Sci.*, Vol. 44, No. 3, 1996, pp. 315–355.

[9]Tillerson, M. and How, J., "Advanced Guidance Algorithms for Spacecraft Formation-keeping," *Amer. Contr. Conf.*, 2002, pp. 2830–2835.

[10]Fiedler, H., Krieger, G., Jochim, F., Kirschner, M., and Moreira, A., "Analysis of Satellite Configurations for Spacebourne SAR Interferometry," *Int. Symp. Formation Flying Missions & Tech.*, Toulouse, France, 2002.

[11]Massonnet, D., "Capabilities and Limitations of the Interferometric Cartwheel," *IEEE Trans. Geosci. and Remote Sensing*, Vol. 39, No. 3, 2001, pp. 506–520.

[12]Schaub, H. and Alfriend, K., "J_2 Invariant Relative Orbits for Spacecraft Formations," *Celest. Mech. Dyn. Astron.*, Vol. 79, 2001, pp. 77–95.

[13]Sedwick, R., Miller, D., and Kong, E., "Mitigation of Differential Perturbations in Formation Flying Satellite Clusters," *J. Astro. Sci.*, Vol. 47, No. 3,4, 1999, pp. 309–331.

[14]Scharf, D., Hadaegh, F., and Ploen, S., "A Survey of Spacecraft Formation Flying Guidance and Control (Part II): Control," *Amer. Contr. Conf.*, 2004.

[15]Berger, L. and How, J., "GVE-Based Dynamics and Control for Formation Flying Spacecraft," *2nd Int. Symp. Formation Flying Missions & Technologies*, Washington, DC, 2004.

[16]Alfriend, K. and Lovell, T., "Error Analysis of Satellite Formations in Near-Circular Low-Earth Orbits," *AAS/AIAA Spaceflight Mech. Mtg.*, 2003, pp. 2349–2371.

[17]Scharf, D., Hadaegh, F., and Ploen, S., "Precision Formation Delta-V Requirements for Distributed Platforms in Earth Orbit," *Enabling Sensor and Platform Technologies for Spaceborne Remote Sensing, SPIE Vol. 5659*, edited by G. Komar, J. Wang, and T. Kimura, 2005, pp. 312–323.

[18]Tillerson, M., Breger, L., and How, J., "Distributed Coordination and Control of Formation Flying Spacecraft," *Amer. Contr. Conf.*, 2003, pp. 1740–1645.

[19]Scharf, D., Ploen, S., Hadaegh, F., Keim, J., and Phan, L., "Guaranteed Initialization of Distributed Spacecraft Formations," *AIAA Guid., Nav.,& Contr. Conf.*, 2003.

[20]Yan, Q., Yang, G., Kapila, V., and de Queiroz, M., "Nonlinear Dynamics, Trajectory Generation, and Adaptive Control of Multiple Spacecraft in Periodic Relative Orbits," *AAS Guid. and Contr. Conf.*, 2000, pp. 159–174.

[21]Vallado, D. and McClain, W., *Fundamentals of Astrodynamics and Applications*, McGraw-Hill, New York, NY, 1997.

[22]Inalhan, G., Tillerson, M., and How, J., "Relative Dynamics and Control of Spacecraft Formations in Eccentric Orbits," *J. Guid., Contr., & Dyn.*, Vol. 25, No. 1, 2002, pp. 48–59.

[23]Prussing, J. and Conway, B., *Orbital Mechanics*, Oxford University Press, New York, New York, 1993.

[24]Fax, J. and Murray, R., "Information Flow and Cooperative Control of Vehicle Formations," *IEEE Trans. Automatic Contr.*, Vol. 49, No. 4, 2004, pp. 1465–1476.

[25]Schweighart, S. and Sedwick, R., "High-Fidelity Linearized J_2 Model for Satellite Formation Flight," *J. Guid., Contr., & Dyn.*, Vol. 25, No. 6, 2003, pp. 1073–1080.

[26]Lewis, F., *Optimal Control*, John Wiley & Sons, New York, New York, 1986.

[27]Lamy, A. and Pascal, S., "Station Keeping Strategies for Constellations of Satellites," *AAS/NASA Int. Symp. on Spaceflight Dyn.*, 1993, pp. 819–833.

[28]Lewis, M. and Tan, K.-H., "High Precision Formation Control of Mobile Robots Using Virtual Structures," *Autonomous Robots*, Vol. 4, No. 4, 1997, pp. 387–403.

[29]Corazzini, T., Robertson, A., Adams, J., Hassibi, A., and How, J., "Experimental Demonstration of GPS as a Relative Sensor for Formation Flying Spacecraft," *J. of the Institute of Navigation*, Vol. 45, No. 3, 1998, pp. 195–207.

[30]Olsen, E., Park, C.-W., and How, J., "3D Formation Flight using Differential Carrier-phase GPS Sensors," *Inst. of Nav. GPS Mtg.*, Nashville, TN, 1998.

[31]Inalhan, G., Busse, F., and How, J., "Precise Formation Flying Control of Multiple Spacecraft using Carrier-Phase Differential GPS," *AAS/AIAA Spaceflight Mech. Mtg.*, 2000, pp. 151–165.

[32]

[33]Bauer, F., Hartman, K., and Lightsey, E., "Spacebourne GPS Current Status and Future Visions," *IEEE Aero. Conf.*, 1998.

[34]Bar-Sever, ed., Y.,, http://www.gdgps.net/system-desc/ index.html, Version of Sept. 23, 2004.

[35]Campbell, M., "Planning Algorithm for Multiple Satellite Clusters," *J. Guid., Contr., & Dyn.*, Vol. 26, No. 5, 2003, pp. 770–780.

[36]Melton, R., "Time-Explicit Representation of Relative Motion Between Elliptical Orbits," *J. Guid., Contr., & Dyn.*, Vol. 23, No. 4, 2000, pp. 604–610.

[37]Tillerson, M., Inalhan, G., and How, J., "Co-ordination and control of distributed spacecraft systems using convex optimization techniques," *Int. J. Robust & Nonlinear Contr.*, Vol. 12, No. 2,3, 2002, pp. 207–242.